One-pot Synthesis of [2+2]-Helicate-like Macrocycle and 2+4-μ_4-Oxo Tetranuclear Open Frame complexes: Chiroptical properties and Asymmetric Oxidative Coupling of 2-naphthols

Eswaran Chinnaraja,[1,2] Rajendran Arunachalam,[1,2] Renjith S. Pillai,[3] Anssi Peuronen,[4] Kari Rissanen[4] and Palani S. Subramanian,*[1,2]

Abstract: Synthesis of binuclear Cu(II) terminally closed [**2+2**]- double-stranded helicate-like macrocycles **1, 1'**,**1"**, **2**, **2'**, **2"** and **2+4-**μ_4-oxo tetranuclear open frame complexes **3**, **3'**, **3"**, **4**, **4'**, **4"** are established. Adapting one-pot self-assembly technique from simple three components systems: 1,1'-binaphthyl-2,2'-diamine, 4-methyl-2,6-diformyl phenol and cupric salts, the helicate-like [**2+2**]- macrocyclic complexes **1 - 1", 2 - 2"** and **2+4-**μ_4-oxo tetranuclear complexes **3 - 3"**, **4 - 4"** were obtained by appropriately altering the reaction condition such as temperature and subcomponent ratio. Density Functional Theory (DFT) calculations were carried out for understanding the structural geometries, intermediates involved in the diverse formation of [**2+2**] and **2+4** frameworks. The single crystal x-ray structures obtained for **1'**, **2** and **3** confirms the self-assembly process in line with DFT. This detailed analysis tempted us to derive a plausible mechanism for this long standing challenge in the synthesis of such macrocycles using 1,1'-binaphthyl-2,2'-diamine (BNDA) and aromatic aldehyde. The chiroptical properties of enantiopure complexes and their catalytic applications in asymmetric oxidative coupling of 2-naphthol to chiral 1,1'-Bi-2-naphthol (BINOL) achieved in good yield and ee were discussed.

Keywords: BINOL, helicate, metal template, macrocycle, self-assembly.

Introduction

Self-assembly,[1,2] the fundamental technique employed by nature to construct well-defined complex superstructures, has gained increasing recognition in recent years. Synthetic supramolecular chemists are yet to understand the controlling factors for the construction of such complex architectures from simple building blocks. The simultaneous formation of covalent –C=N (carbon-hetero atom) and dative (O-M or N-M) bonds in Schiff base ligand and its complexes, allow to obtain varieties of highly complex macrocycles with various sizes of voids.[3] In metallo-supramolecular chemistry, the process of selective binding between metal ions and appropriate ligands leads to the formation of organized structures such as helicates[4] and knots[5] used in different applications.

Gao et al.[6] have reported the synthesis of a series of macrocycles containing N_4O_2 cavity incorporating 4-methyl-2,6-diformylphenol (4-MDFP) and diamines as building blocks. While they were successful in the synthesis of various macrocycles by adopting diamines such as ethylenediamine (en), (1*R*,2*R*)-diaminocyclohexane (*RR*-DACH), and (1*R*,2*R*)-diphenylethylenediamine (*RR*-DPEN), they also reported their unfruitful attempts in the case of binaphthyldiamine (BNDA) with 4-MDFP. Although their study was limited to Ni^{2+} complexes, the structural rigidity or axial chirality of the BNDA were believed as restricting factors for not obtaining the desired [**2+2**]-macrocycle.

Scheme 1. Metal-templated synthesis of macrocycles.

The preparation of [**2+2**]-macrocycle from BNDA and 4-MDFP has, thus far, remained a challenge. Understanding the structural significance on such BNDA based macrocycles in host-guest chemistry,[7] chiral recognition,[8] and asymmetric catalysis,[9] we inspired here to re-explore the synthesis of BNDA derived system[6,10] by adopting the 4-MDFP as building block with appropriate modification in the synthetic strategy.

Scheme 2. Synthesis of terminally closed double stranded [**2+2**]-helicate by the different template method

In our recent report[11] described the successful synthesis of such BNDA based [**2+2**]-helicates by one-pot metal (copper (II), zinc (II)) template techniques and the failure of Gao et al. in such attempts we inspired to investigate the mechanism behind the synthetic strategy by playing with the subcomponents. Hence, in the present study demonstrate the synthetic viability for the formation of [**2+2**]-terminally closed double-stranded helicate-like macrocycle using subcomponents self-assembly techniques. In this important step, expanding the understanding on this area of research, we have also, isolated an intermittent **2+4** species with a μ_4-oxo tetranuclear[12] open framework (complex **3**) and characterized by single crystal X-ray.

[1] *Inorganic Materials and Catalysis Division, Central Salt and Marine Chemicals Research Institute (CSIR-CSMCRI), Bhavnagar, 364002, Gujarat (India).E-mail: siva@csmcri.res.in*

[2]*Academy of Scientific and Innovative Research (AcSIR), Ghaziabad 201002, India.*

[3] *Department of Chemistry, SRM Institute of Science and Technology, Kattankulathur- 603203, Tamil Nadu, India.*

[4]*Department of Chemistry, Nanoscience Center, P.O. Box 35, FI-40014, University of Jyvaskyla, Jyväskylä, Finland.*

Results and Discussion

In the course of synthesis of [**2+2**] assembly, four different approaches were attempted. These include direct addition of dialdehyde and BNDA (i), templating through boric acid (ii), phenylboronic acid (iii) and metal salts template (iv) (Scheme 2). In the case of (i), the direct mixing of either *tert*-butyl-2,6-diformylphenol or 4-methyl-2,6-diformylphenol with BNDA refluxing in ethanol (Scheme 2-ia & Figure S1) and RT in methanol (Scheme 2-ib & Figure S2) for 36 h resulted in a mixture showing a complicated m/z pattern in the positive ion MS mode. This indicates the existence of all different combinations except the desired [**2+2**] species. Following our recent report,[13] where we have demonstrated the successful synthesis of a similar [**2+2**] macrocycle from DPEN and 3,3′-methylene-bis(5-(*tert*-butyl)-2-hydroxybenzaldehyde, we implemented the procedures (ii) and (iii), that employ boric acid [Scheme 2-ii(a)-ii(b)] and phenylboronic acid (Scheme 2-iii) as templating reagents. However, in the case of BNDA and 4-MDFP, all these methods (i-iii) produce complicated MS patterns with numerous peaks attributable to **1+1** (m/z = 431.36), **2+1** (m/z = 647.52), **1+2** (m/z = 697.37, a negligible population of [**2+2**]-macrocycle (m/z = 825.47) and **3+2** (m/z = 989.51) species (Figure S1-S5). Also the consequent ^{1}H NMR spectra being highly complex suggest that as a mixture of several Schiff base products. Hence, to briefly summarize, none of the above procedures (i)-(iii) produced the desired [**2+2**] species exclusively (Scheme 2). The formation of negligible amount of [**2+2**] product and the associated difficulties in the separation of the

mixture, demanded us to revise our synthetic strategy. Accordingly, a simplified synthesis method (iv), where the metal salts has been used as templating reagent (Scheme 2-iv), was established. In this procedure, copper (II) salt was first added to a NEt_3-treated dialdehyde 4-MDFP, which gives a colour change from yellow to green. Addition of BNDA to this solution with constant stirring at RT exhibited an increasingly intense green colour during the course of the reaction. This **2:2:2** acetonitrile mixture of dialdehyde:metal:diamine was refluxed for 36 h. During this long reaction time, the dark green solution changed slowly into dark brown. Evaporation of the solution under reduced pressure provided a solid residue, which was treated with CH_2Cl_2/H_2O mixture. The organic layer was separated and dried. To our surprise, this method is highly selective and provides the [**2+2**] complex as a sole product as shown in scheme 2(iv).

Following the success of this one-pot metal template method (iv), we have carried out two separate reactions to synthesis two [**2+2**] dinuclear double-stranded helicates, **$[Cu_2(L_a^{rac})(OAc)_2]$**, **1** and **$[Cu_2(L_a^{RR})Cl_2]$**, **1'**, respectively, in good yields (ca. 80-85%) using 4-MDFP (pre-treated with NEt_3 to facilitate deprotonation of the phenol group) and two different Cu(II) sources, $Cu(CH_3COO)_2{\cdot}H_2O$ or $CuCl_2{\cdot}6H_2O$, followed by addition of *rac*-BNDA or *R*-BNDA respectively with appropriate ratios (S2). The ESI-MS spectra of complex **1** (derived from copper(II) acetate, Figure S6) and complex **1'** (derived from copper(II)chloride, Figure 1 and Figure S7) show single dominant peak of the respective [**2+2**] binuclear metallohelicates at m/z = 1007.43 and 983.65, respectively, which match well with their monocationic ions [**1**-OAc]$^+$ (Calc: 1007.85) and [**1'**-Cl]$^+$ (Calc: 983.13). The gas phase analyses thus unequivocally establish a neat formation of the desired [**2+2**] assemblies (Figure 1).

Figure 1. ESI-MS spectra of **$[Cu_2(L_a^{RR})Cl_2]$** (**1'**)

Figure 2. Illustration of the X-ray crystal structure of [**2+2**] **$[Cu_2(L_a^{RR})Cl_2]$** complex **1'** (disordered atoms and solvent molecules are omitted for clarity). Thermal ellipsoids are presented at 30% probability level. Symmetry operation (') equals to (x, 1-y, 1-z).

Further evidence on the successful formation of the [**2+2**] product **1'** was provided by single crystal X-ray analysis. Crystals of **1'** were obtained as acetonitrile solvates after a couple of weeks of slow evaporation of CH_3CN solution. The crystal structure of **1'** was solved in a non-centrosymmetric space group $C222_1$ with four molecules of **1'** in the unit cell (Z' = 0.5).[14] The structural analysis shows a neutral binuclear double-stranded Cu(II) helicate complex, which possesses two binaphthyl diamine and two 4-MDFP units that incorporate two Cu(II)–Cl centers, *viz.* **$[Cu_2(L_a^{RR})Cl_2]$** (Figure 2). The macrocyclic ligand (L_a^{RR}) in **1'** possesses two metal binding domains, each consisting of an N_2O_2 chromophoric compartment with two azomethine nitrogens, N1 and N2, [*d*(Cu1–N1) = 2.078(4)Å, *d*(Cu1–N2) = 1.940(4)Å] and two phenolic oxygens, O1 and O2 [*d*(Cu1–O1) = 1.916(2) Å and *d*(Cu1–O2) = 2.033(3) Å]. These central phenolate oxygens bridge the Cu(II) centers and form a planar Cu_2O_2 core as shown in Figure 2. Thus, each Cu(II) ion adopts an identical distorted square pyramidal geometry by coordinating to two azomethine nitrogens and two phenolate oxygens with the Cu atom sitting 0.48 Å above the square base and a chloride ion at the apex.

The relevant bond distances and angles are presented in Table S1. The axially chiral BNDA units, incorporated in the (L_a^{RR}) backbone coordinate to the Cu-atoms via their azomethine nitrogens and are twisted in an angle of ca. 72° in respect to the biphenyl planes. Additionally the DFT optimization

performed for complex **1** re-establish the structure as reveal that the metal binding domain retains the planar Cu_2O_2 core, where the Cu(II) centers are bridging through the phenolate oxygens (Figure S15c). This energy minimized structure have revealed the metal binding with two azomethine nitrogens, N1 and N2, (*d*(Cu1–N1) = ≈2.049 Å, *d*(Cu1–N2) = ≈1.971 Å] and two phenolic oxygens, O1 and O2 [*d*(Cu1–O1) = 1.979 Å and *d*(Cu1–O2) = 2.089 Å] on matches to its single crystal x-ray structure obtained for **1'**.

Consolidation of the above analysis suggests that the boric and phenylboronic acid templates are not efficient methods for the synthesis of the [**2+2**] macrocycle. In contrast, the metal templated approach (iv) [Scheme 2-iv] gave the [**2+2**] product selectively and, thus, proved to be highly efficient for its preparation. Furthermore, the helically twisted conformation of **1**, **1',** illustrates that the metal has a vital role in the construction of the ligand $\mathbf{L_a}$. This observation indicates that metal chelation is a dominant factor in the self-assembly, whereas the axial chirality and the structural rigidity hinder the formation of the [**2+2**] species. In other words, metal chelation – in combination of other parameters such as reaction time and temperature – promotes the selective formation of the [**2+2**] complex and reveals the preparation of this ligand without metal ion is nonselective. Similar procedure adopted for the synthesis of complexes **2**, **2'**, **2"** containing $\mathbf{L_b}$ ligand as shown in scheme 1.

The **2:2:2** ratio of metal:aldehyde:amine mixture, stirring at room temperature has resulted a **2+4** - open frame work of μ_4-oxo-tetranuclear complex **3** (Scheme S1). This appealing structure, of complex **3** obtained from **2:2:2** ratio at room temperature surprised us. When we used **2:2:2** ratio, this complex existing with two diamines, two metals, but one dialdehyde inspired us to investigate the role of subcomponents ratio. Hence adapting a minor change in the subcomponent ratio in order to achieve high selectivity for complex **3** was attempted. Accordingly, with **2**:**4:4** ratio of 4-MDFP+NEt_3, $Cu(CH_3COO)_2 \cdot H_2O$ and *rac*-BNDA in acetonitrile solution found to form $\mathbf{L_c}^{rac}$ (Scheme 1) which is present as a **2+4** complex **3.** This tetrameric Cu(II) assembly **[$Cu_4(\mu_4$-O)($\mathbf{L_c}^{rac}$)$_2(\mu_2$-OAc)$_4$]** (**3**) built around a μ_4-oxo ion, could be systematically and repeatedly produced with 80% yield (S3). The MS spectrum of **3** show a dominant peak at m/z = 1838.43 corresponding to monocation [**3-OAc**]$^+$ (Calc: 1838.32, Figure S8) and confirms the formation of **2+4**, μ_4-oxo–tetramer comprising two 4-MDFP and four BNDA. In the case of **2:4:4** ratio, one of the two amines of each BNDA moiety undergoes Schiff base condensation with 4-MDFP, while the other amine of BNDA remains unreacted. Thus both aldehydes of 4-MDFP undergoing Schiff base condensation, each ligand of ($\mathbf{L_c}^{rac}$) contains two azomethine and two primary amine groups as shown in Figure 3a.

Figure 3. (a) Single crystal x-ray structure of complex **3,** (b) Magnification of the inner core, **[$Cu_4(\mu_4$-O)($\mathbf{L_c}^{rac}$)$_2(\mu_2$-OAc)$_4$]**. Disordered atoms and solvent molecules are omitted for clarity. Thermal ellipsoids are presented at 30 % probability level. Symmetry operation (') equals to (-x, y, 0.5-z). Here shown only **[$Cu_4(\mu_4$-O)($\mathbf{L_c}^{SS}$)$_2(\mu_2$-OAc)$_4$]**-enantiomer and the counterpart **[$Cu_4(\mu_4$-O)($\mathbf{L_c}^{RR}$)$_2(\mu_2$-OAc)$_4$]**-enantiomer is removed for clarity.

Dark green crystals of **3** were obtained in 10-15 days upon slow evaporation of its acetonitrile solution. The structure was solved in a centrosymmetric monoclinic space group *C*2/*c* with four molecules in the unit cell (*Z*' = 0.5) accompanied by acetonitrile solvent molecules.[15] X-ray structural analysis (S4) shows that the complex is composed of two ($\mathbf{L_c}^{rac}$) ligands, each of which incorporates two Cu(II) ions using the azomethine nitrogen atoms as terminal sites and the phenolate oxygen as a bridging atom, thus resulting in

an "N–Cu–O–Cu–N" unit (Figure 3b). Two of these $Cu_2(\mathbf{L_c}^{rac})$ units are coupled together by four acetate ions (in a *syn-syn* mode) and a O^{2-} ion to generate the complete **$[Cu_4(\mu_4\text{-}O)(\mathbf{L_c}^{rac})_2(\mu_2\text{-}OAc)_4]$** neutral complex, with a cage-like Cu_4O core, where O_2^{2-} exists in a tetrahedral arrangement. Each of these Cu-atoms are thus coordinated to one azomethine N-atom and one phenolate O-atom of the ($\mathbf{L_c}^{rac}$) ligand, two O-atoms of two distinct acetate anions and the central O^{2-} to yield an approximate square pyramidal coordination environment. The average Cu–O2 bond distance is 1.92 Å whereas the Cu–O–Cu angles vary between 102.4° (Cu1–O2–Cu2) and 124.7° (Cu1–O2–Cu1'). The X-ray structure analysis confirms that, amongst the two amine groups of each BNDA moiety, only one undergoes a condensation to form an azomethine (N3, N4A/B). Hence, complex **3** consists of two ($\mathbf{L_c}^{rac}$), both of which contain two amine groups, and thus a total four amine groups remain dangling in each complex unit and are directed toward the O-atoms of the bridging acetate ions [*d*(N-O) = 3.03-3.78 Å]. As a result, the twisting of the biphenyl rings of the BNDA moieties are not restricted by covalent or dative bonding scaffold (*cf.***1'**). Regardless, the twisting angle of ca. 74.5-76.6° is similar to that observed for **1'**. The DFT optimized structure of complex **3** (Figure S15d) also confirms that two $Cu_2(\mathbf{L_c}^{rac})$ units are coupled together by four acetate ions (in a *syn-syn* mode) and a O^{2-} ion to generate the complete **$[Cu_4(\mu_4\text{-}O)(\mathbf{L_c}^{rac})_2(\mu_2\text{-}OAc)_4]$** neutral complex. A similar method adopted to obtain enantiopure version of complex **3** such as **3'**, **3"** by using R-or S-BNDA respectively (Figure S9 and Figure S10) were successful.

Figure 4. Molecular structure and partial atomic numbering scheme for the $[Cu_4(\mu_4\text{-}O)(\mu\text{-}COOCH_3)_4(L_d^{rac})_2]$ **4** . Hydrogen atoms are omitted for clarity. Here shown only **$[Cu_4(\mu_4\text{-}O)(\mathbf{L_d}^{RR})_2(\mu_2\text{-}OAc)_4]$**-enantiomer and the counterpart **$[Cu_4(\mu_4\text{-}O)(\mathbf{L_d}^{SS})_2(\mu_2\text{-}OAc)_4]$**-enantiomer is removed for clarity.

Changing 4-MDFP by 4-tBDFP (4-tert-Butyl-2,6-diformylphenol) in the subcomponent produce complex **4**. Complex **4** upon slow evaporation of acetonitrile solution crystallized in monoclinic crystal system with C2/c space group.[16] The molecular structure of the complex **4** is shown in Figure 4. Selected bond distances and bond angles are listed in table S1. This neutral molecule composed in a tetrameric copper assembly with two monoanionic Schiff base ligands (L_d^{rac}), one μ_4-oxide ion and four-acetate bridge. Each ligand (L_d^{rac}) binding Cu1 and Cu2 with azomethine nitrogens (N1, N2) forms a dimer, bridging through phenolate oxygen (O1) of central cresol moiety. Two such dinuclear L_d^{rac}[Cu1-Cu2] units perpendicular to each other in their plan are bridged through four COO group of acetate ion. All four Cu(II) centers thus forming a cage type paddle wheel structure is framed by acetate bridge, a μ_4-oxide ion is trapped inside the cage as shown in Figure 4. The oxygen atom sitting at the center, all four Cu(II) ions occupies the corners of the tetrahedral geometry with a bond distance dCu1-O2 = 1.932 and dCu2-O2 = 1.911 Å. The μ_4-oxo tetrahedral geometry is established with the *trans* angles <Cu2-O2-Cu2 = 104.70° and <Cu1-O2-Cu1 = 107.73° and the *cis* angle are in the range of 103.57-119.07°. The Cu1 center in the dimeric unit coordinating with phenolate oxygen O1, O3 of acetate ion, O2 of oxide ion and azomethine N1 forms a square base, while the O4 of the acetate oxygen involved in apical coordination (Cu1-O4 = 2.298 Å). The square pyramidal geometry of [Cu1-O1 = 2.000; Cu1-N1 = 1.990; Cu1-O2 = 1.911; Cu1-O3 =1.953; Cu1-O4 = 2.298Å]. similarly the Cu2 center forms square base with phenolate O1, O5 of acetate ion, O2 of oxide ion and azomethine N2 while the O5 of acetate oxygen involves in apical coordination (Cu1-O5=2.303Å) with comparatively longer bond distance. Both Cu1 and Cu2 sitting almost in the same plane (12.17°) moved little up from their square base by 0.193 Å and 0.184 Å respectively towards their apical coordination. Amongst two amine group in the binaphthyl moiety one involves in condensation and forms azomethine while the other is free. Each

biphenyl rings within the binaphthyl moiety are twisted almost perpendicular to each other with an angle ranging 77.59°-84.21° reveals axial chirality. The detailed analysis of the H-bonding interaction suggests that one molecule of acetonitrile from each side the cyanide nitrogen through NH…N and CH…N interaction is guided from top and bottom cleft. Similarly the enantiopure version of the complex **4** such as **4'** and **4"** were also synthesised (Figure S12 and Figure S13).

Figure 5. UV-vis spectra of all complexes **3 - 3"** and **4 - 4"** in THF ($1x10^{-5}$M). The inset shows the d-d band ($1x10^{-3}$M).

Electronic spectra of all these complexes exhibit an almost similar spectral patterns with the *d-d* band at 665±5 nm and the ligand-centered transition at 247±5, 267±5, 288±5 nm (Figure 5) thereby confirming the complexation with Cu(II). The peaks at 400 – 430 nm corresponds to LMCT transition from the phenolate oxygen to Cu(II). The *d-d* bands at 665±5 nm for all the complexes suggest a distorted square pyramidal geometry, which matches with the corresponding crystal structures (Table S2). The FT-IR spectra depicting an intense band at ≈1615 cm^{-1} are attributed for the C=N stretching frequency in all the complexes thus confirm the formation of azomethine bond.

Figure 6. Circular dichroism (CD) spectra for the complexes **3'**, **4'** and their enantiomeric counterpart **3"**, **4"** recorded in THF ($1x10^{-5}$M). The inset shows the d-d band ($1x10^{-3}$M).

The chiroptical properties of complexes were investigated by circular dichroic (CD) spectroscopy. The chiroptical properties of [**2+2**] helicates **1'**, **1"**, **2'**, **2"**were studied extensively in our recent report.[11] The CD spectra (Figure 6) of complexes **3'**, **4'** and **3"**, **4"**depicting similar but exactly opposite pattern demonstrates their enantiopurity. The ligand centred transition and LMCT in CD spectra at 249, 295 and 401 nm of complexes show similar pattern with opposite cotton effect suggesting the enantiomeric nature of the complexes. The opposite CD pattern suggest that, the chirality of the ligand transferred to metal centre to form *ΛΛΛΛ* in complexes **3'**, **4'** while *ΔΔΔΔ* chirality at metal centre in complexes of **3"**, **4"** respectively.[17] The *RR*-isomer of binaphthylamine ligand transfers their chirality to Cu(II) and the respective tetranuclear complex thus gains *ΛΛΛΛ* geometrical chirality around Cu(II) center. Similarly the opposite enantiomer in the same complex generates *ΔΔΔΔ* form as observed in the case of [**2+2**]-helicates such as *ΛΛ*-**1'**, *ΔΔ*-**1"**, *ΛΛ*-**2'**, *ΔΔ*-**2"**.

The crystal structures of **1', 3** and **4,** suggests that the BNDA in them exhibit a self-sorting[18] behaviour; A similar complex reported[11] by us recently have been illustrated to follow a similar self-sorting behaviour based on their chirality. Possessing BNDA a similar situation in the present complex **$[Cu_2L_a^{RR}.Cl_2]$, 1'** inspired us to investigate its role of chirality followed in the self-assembly process. Having used the enantiopure *R*-BNDA, in complex **1'** there would not be any surprise to obtain enantiopure complex **$[Cu_2L_a^{RR}.Cl_2]$** in the unit cell (Figure S14).

1). Self-sorting phenomenon in complex **1'**

$$2(\text{4-MDFP}) + 2MX_2 + 2\text{-}(R\text{-BNDA}) \longrightarrow \Lambda\Lambda\text{-}[M_2L_a^{RR}X_2] + 2X_2 \quad \text{.....eq.1}$$

2). Self-sorting phenomenon in complex **3, 3', 3''**

$$2(\text{4-MDFP}) + 4MX_2 + 4\ (rac\text{-BNDA}) \longrightarrow \Lambda\Lambda\Lambda\Lambda\text{-}\tfrac{1}{2}[M_4(\mu_4\text{-}O)(L_c^{RR})(\mu_2\text{-}OAc)_4] + \Delta\Delta\Delta\Delta\text{-}\tfrac{1}{2}[M_4(\mu_4\text{-}O)(L_c^{SS})(\mu_2\text{-}Ac)_4] + X_2 \quad \text{.....eq.2}$$

$$2(\text{4-MDFP}) + 4MX_2 + 4\ (R\text{-BNDA}) \longrightarrow \Lambda\Lambda\Lambda\Lambda\text{-}[M_4(\mu_4\text{-}O)(L_c^{RR})2(\mu_2\text{-}OAc)_4] + X_2 \quad \text{.....eq.3}$$

$$2(\text{4-MDFP}) + 4MX_2 + 4\ (S\text{-BNDA}) \longrightarrow \Lambda\Lambda\Lambda\Lambda\text{-}[M_4(\mu_4\text{-}O)(L_c^{SS})2(\mu_2\text{-}OAc)_4] + X_2 \quad \text{.....eq.4}$$

Most surprisingly the racemic BNDA used in complex **3,** found to produce both homochiral complexes **$[Cu_4(\mu_4\text{-}O)(L_c^{RR})_2(\mu_2\text{-}OAc)_4]$** and **$[Cu_4(\mu_4\text{-}O)(L_c^{SS})_2(\mu_2\text{-}OAc)_4]$** in the unit cell (Figure S15). Our analysis in the present structure obtained for complex **3** did not show any heterochiral formation such as **$[Cu_4(\mu_4\text{-}O)(L_c^{RR})(L_c^{SS})(\mu_2\text{-}OAc)_4]$, $[Cu_4(\mu_4\text{-}O)(L_c^{RR})(L_c^{RS})\ (\mu_2\text{-}OAc)_4]$, $[Cu_4(\mu_4\text{-}O)(L_c^{RS})(L_c^{SR})(\mu_2\text{-}OAc)_4]$** etc**.** Similarly the racemic complex **4** also show a self-sorting phenomenon by evolving two independent units **$[Cu_4(\mu_4\text{-}O)(L_d^{RR})_2(\mu_2\text{-}OAc)_4]$** and **$[Cu_4(\mu_4\text{-}O)(L_d^{SS})_2(\mu_2\text{-}OAc)_4]$** in the unit cell (Figure S16). To further simplify the homochiral process in the complex **1**, **3** and **4** the equation 1 and 2 above defines the formation of respective isomers in the single crystal structure and the enantiopure complexes in equation 3 and 4.

Figure 7. (a) X-band EPR spectra of **1** and **3** in liq.N_2 (90K, DCM); (b) Solid state EPR spectra of **1** and **3** at RT.

Considering the dimeric and tetrameric Cu(II) association, we inspired to record the EPR spectra of the complexes in both solution (Figure 6a) and solid state (Figure 6b). The EPR spectra at frozen temperature using liquid nitrogen in solution state reveals a partially merged parallel and perpendicular features as shown in Figure 7a. All these complexes in their solution state at room temperature (Figure S17) and at frozen temperature (Figure 7a, Figure S18 & Figure S19) provide a weak spin forbidden transition $\Delta ms = \pm 2$ at g = 4.30 to 4.40. This observation confirms their dimeric, tetrameric association and reveal a strong M-M interaction as reported in the literature.[19] The dimeric complex **1** in frozen DCM solution gives a partially resolved parallel and perpendicular features with $g_{II} = 2.43$, $g_{\perp} = 2.07$ and $A_{II} = 167G$. In all these complexes, the measured A_{II} lies in the range 165G±2G in their frozen temperature spectra. In the case of solid state EPR, the broad resonances (Figure 7b) illustrate a strong influence of dipolar broadening. The ΔH_{pp}, measured for complexes **1** and **3** in their solid state room temperature spectra (Figure 7b), are 172G, and 318G respectively and suggests the line broadening in **3** > **1**. This reflects their dipolar broadening and the consequent M-M interaction in their solid state mediated through various exchange pathways such as i) $Cu\text{-}O_{(phenolate)}\text{-}Cu$, (ii) $Cu\text{-}OCO_{(acetate)}\text{-}Cu$, (iii) $Cu\text{-}O_{(peroxo)}\text{-}Cu$ in the complexes. In the case of complex **1,** the closely packed ring structure, the M-M interaction is expected to be stronger, whereas in the open frame structure **3**, the dipolar interactions seems to be dominant. The similar behavior also observed for all other complexes such as **2** and **4**.

With the above understanding obtained from the structure, EPR, UV-Vis and CD studies, we propose a mechanism, accordingly supramolecular self-assembly processes – leads to the formation of [**2**+**2**] complex **1** and **2**+**4** species **3** all of which are described in this work (Scheme 3). We suggest that in the initial step of the metal template synthesis, *i.e.* the mixing of 4-MDFP with an equivalent ratio of copper(II) salts,

generates an intermittent tetra-aldehyde complex (intermediate-1 in Scheme 3), which is facilitated by base-induced deprotonation of 4-MDFP and consequent formation of the phenolate anion. Formation of such dialdehyde species is supported by the earlier work of Alzu et *et al*.[20] who report the X-ray structure of $[Cu_2(4\text{-}MDFP)_2(ClO_4)]$ – a perchlorate salt analogue of the proposed intermediate-1 (**Int-1**). This structure shows that in the bimetallic $Cu_2(4\text{-}MDFP)_2$ system, the aldehyde groups are brought into close proximity and the two phenolate backbones are in a planar conformation with the Cu-coordinated anions *trans* to each other as shown in **Int-1** in scheme 3. *In situ* condensation between this aldehydes at C**1**, C**7** and C**1'**, C**7'** with BNDA in **Int-1** can then follow two different pathways through step 1 and 2. If the opposite aldehydes C**1**, C**7'** or C**1'**, C**7** react with two different BNDA, the complex undergoes *trans* condensation *via* step 1 and generates a semi-Schiff base intermediate **Int-2**, that under refluxing at 80°C for 36h reaction time forms a binuclear double-stranded terminally closed helicate **1** and **1'** *via* successive condensation as shown in step 1a. The long reaction-time and the 80°C reflux as mentioned in the synthetic procedure are considered essential to achieve this of terminally closed helicate; otherwise this [**2+2**] complexation would not have been possible to achieve is understandable.

Alternatively, *cis* condensation, through step 2, where the Schiff base formation takes place at C**1**, C**7** or C**1'**, **7'** positions, with two different BNDA, would promote the formation of **Int-4** species, *via* another intermediate-3 *(***Int-3**) *i.e.*$[Cu_2\mathbf{L_c}(OAc)_2(\mu\text{-}OH)]$, in which one of the two dialdehyde species remain unreacted. The path from **Int-3** to complex **3** is more complicated to predict, but one plausible mechanism would be that the involvement of protonation of the phenolate ion 4-MDFP from water and then consequent formation of a hydroxide complex,[21] as shown in **Int-3** $[Cu_2\mathbf{L_c}(OH)(OAc)_2]$. Coupling of two such hydroxide species, **Int-3** $[Cu_2\mathbf{L_c}(OH)(OAc)_2]$, would then result in the formation of μ_4–oxo ion centered species **Int-4** as shown in step 2a leaving one water molecule. Then the intramolecular rearrangement of acetate in **Int-4** may lead to complex **3** as shown in Scheme 3.

Scheme 3. A plausible mechanism for the formation of complexes **1-3** (M = Cu(II), X = counter ion)

The described syntheses and consequent analyses of the complex **1-3** show that the appropriate tuning of the ratio of the subcomponents, 4-MDFP with copper(II) salt and BNDA, and reaction conditions, affords a diverse metal complexes: [**2+2**]-helicates (**1** and **1'**), tetrameric **2+4-**open frame complex **3**. Although both these steps require careful control over the reaction temperature and subcomponents ratio, the described method is highly selective and gives pure products in good yields, and thus provide a convenient pathway to the diverse complex formation reported presently. The formation of [**2+2**] system also show that, in addition to the M:L subcomponent ratio, the temperature and choice of order of subcomponents (dialdehyde followed by metal salt and then diamine) also play a significant role in the self-assembly of the desired product.

The diversity in the formation of complexes **1** and **3** by appropriately tuning the ratio of the similar subcomponents as mentioned above inspired us to investigate the probable mechanism based on the geometry optimization using computational calculations for all the complexes and intermediates. These complexes **1** and **3** are optimized using standard DFT module(S5).The proposed **Int-1** was initially optimized and this bimetallic $[Cu_2(4\text{-}MDFP)_2]$ system undergoes condensation between aldehydes and BNDA in two different pathways as shown in the scheme 3. The opposite aldehydes in the **Int-1** react with

two different BNDA *via trans* condensation and generates a semi-Schiff base intermediate **Int-2**, which on refluxing at 80°C for 36h reaction time forms a binuclear double-stranded terminally closed complex **1** (step 1a). The relative free energy ≈89 kcal mol^{-1} of the **Int-2** (Figure 8) obtained through computational study thus strongly suggests that the formation of complex **1** would be possible, only with the supply of a high energy such as reflux in 80°C in the present case for 36h. It is obvious to understand that this reaction is highly endothermic and that is why the earlier attempts were ended unsuccessful. The axial chirality and the structural rigidity caused by the BNDA in the complex **1** thus actually requires such a high amount of energy to afford the [**2+2**] metal directed self-assembly. The crystal structure of complex **1'** also clearly dictating the formation of [**2+2**] assembly matches well with the computational results. The requirement of high amount of energy ≈89 kcal mol^{-1} and long reaction time of 36 h was not met in the earlier reports. On the other hand, the *cis* condensation with two different BNDA would led to form **Int-4** through **Int-2.** In absence of reflux, the mechanism leads to form the thermodynamically stable complex **3**. This following step 2, one among the two dialdeyhyde (2-MDFP) species is expected to remain unreacted which in-turn involves in promoting the hydroxide species. The optimized **Int-4** shows the favourable chelation of Cu(II) with the acetate anions with minimal free energy (≈8 kcal mol^{-1}). Therefore, the formation of **Int-4** requires small amount of energy compared to **Int-2** and hence it is much easier through this intermediates as shown in scheme 3 and Figure 8. A coupling of two such **Int-2** species would then result in the formation μ_4–oxo ion centered complex **3** as shown in step 2 (Scheme 3). The relative free energy of all these species calculated using computational studies for **Int-1**, **Int-2**, **Int-3**, **Int-4**, complex **1** and **3** are plotted in Figure 8. The crucial step in the whole mechanism is being the formation of two different intermediates, **Int-2** and **Int-4**, both are analyzed using DFT studies (Figure S20) which supports that the proposed mechanism in the scheme 3 is very much feasible through this synthetic approach. In addition to DFT studies, we have also attempted to identity both the **Int-2** (Figure S21) and **Int-3** (Figure S22) by mass analysis. Accordingly the occurrence of monocationic species of **int-3** at m/z = 939.2176 [Calc = 939.17] and dicationic species of **int-2** at m/z = 984.9686 [Calc = 984.18] supports the formation of such species. Both the analysis were carried out after the addition of BNDA to **Int-1**. The **Int-3** was identified upon using **2:4:4** ratio and **Int-2** was identified from **2:2:2** ratio mixture.

Figure 8. The relative free energy all the species (**Int-1**, **Int-2**, **Int-3**, **Int-4**, complex **1**, **3**) calculated using computational studies. Insert the intermediates isolated for complexes **1-3.** (M = Cu(II), X = acetate ion) (Distances in the molecular structure are in Å).

The detailed study dictating two different mechanistic pathways, the diversity in the complexation thus suggests very interesting findings. The step 1 through which the [**2+2**] formation of complex **1** & **1'**, being end-product, requires large amount of endothermic energy. As supported by the DFT study the relative free energy ≈89 kcal mol^{-1} and ≈87 kcal mol^{-1} for **Int-2** and complex **1** are very much convincing with the reaction condition. The other approach following through step 2 leading to form complex **3** through **Int-4**, at RT provide the **2+4**-open framework. The complex **3** with **2+4**-open framework being promising species provides opportunity to construct diverse macrocyclic compounds with variable voids and sizes through further Schiff base condensations.

Catalysis

Inspired from the chiroptical properties, we aimed to investigate these complexes on enantioselective catalysis. Accordingly we used them as catalysts in the C-C coupling reaction of 2-naphthol to BINOL. In general oxidative coupling involving C-C bond formation reactions are studied using various chiral amine copper complexes,[22] iron complexes,[23] and vanadium complexes as catalysts.[24] In general, the catalytic system in oxidative coupling reaction is efficient in the presence of oxygen source.[25] Hence in an attempt to understand their catalytic capability, we used them as oxidation catalyst in aryl-aryl coupling reactions. With this in mind, all the complexes were adapted as catalysts for the conversion of 2-naphthol to enantioselective *R* and *S*-BINOL.

Table 1: Screening of catalyst and oxidising agent[a]

[a] All reactions were carried out using 0.5mmol substrate, 3mL of solvents for 72 h. [b] Isolated yield, [c] er and ee were calculated by HPLC profile using Lux cellulose-1 column. Configuration of the product was assigned by comparing with HPLC profile of reported. [d] t-BuOOH in H2O. [e] t-BuOOH in decane

Initially, the [**2**+**2**]-helical complexes **1, 1'** and **2, 2'** were adopted as catalyst for this reaction in presence of atmospheric air, DCM, RT and 1 mol% catalyst as reaction condition. The progress of the reaction was monitored following the consumption of the substrate using TLC. The complexes **1** & **2** being racemic in nature, it is not surprise to obtain racemic BINOL as product (Table 1, entry 1 & 3). Unfortunately the yield is found to be very low 20 - 23%. Hence adapting their enantiomeric counterparts **1'** and **2'**, this reaction produced BINOL of poor yield of 25-26% with ee 12 & 10 % was not encouraging (Table 1 entry 2 & 4). Hence, we used the open frame complex **3** as catalyst, which produced comparatively better yield of 50% (Table 1, entry 5). We then used the enantiopure form of open frame complex **3'** for the conversion of 2-naphthol, which produced BINOL with 52% yield and 20% ee (Table 1, entry 6). In the presence of atmospheric air as oxidising agent, the reaction produced mixture of products rather than single product of BINOL. Henceforth we screened various oxidizing agent as shown in the table 1, entry 7-11.

Various oxygen sources such as di-tertiary butyl hydrogen peroxide (Table 1, entry 7), tertiary butyl hydrogen peroxide in water (Table 1, entry 8), and tertiary butyl hydrogen peroxide in decane (Table 1, entry 9) hydrogen peroxide (Table 1, entry 10) were adapted. In all these case, the ee of the BINOL obtained was in the range, ≈2 to 12% and the yield ranges ≈54 to 60%. Replacing the atmospheric oxygen by pure oxygen, the reaction failed to make any desired change but resulted into the formation of many by-products. Since change in the oxygen source is not making any significant improvement in the yield and ee (Table 1, entry 11), all further optimisation were carried out without external oxygen supply. There are significant number of reports on chiral amine and copper catalysed oxidative coupling reactions without using oxygen source,[26] since copper amine itself is acting as an oxidising agent in such reaction. Interestingly, the complex **3** containing both amine and metal centre, the tetranuclear complexes reported in this manuscript trapping oxide ion in its tetrameric cage, the structural features inspired us to use this as catalysts. Although few such μ_4-oxo-tetranuclear complexes have been already reported,[12] so far the researchers were interested on its structural features but not explored their catalytic activity in-particular in the oxidative C-C bond coupling of 2-naphthol.

Table 2: Solvent variation[a]

[a] All reactions were carried out using 0.5mmol substrate, 3mL of solvents for 72 h. [b] Isolated yield, [c] er and ee were calculated by HPLC profile using Lux cellulose-1 column.

The advantage of using copper amine complexes, is that catalyse the reactions in very mild reaction condition and leads mainly to the formation of the BINOL as major product. To our surprise, the present reaction when performed without any external oxygen source (Table 1, entry 12) found to give better yield as 74% and moderate enantioselectivity (30% ee). In a similar condition (Table 1, entry 13), we adopted for catalyst **3"** of opposite isomer of catalyst, which gave almost similar result (75% yield and 32% ee), with opposite configuration. Similarly the catalyst **4**, **4'** and **4"** were checked for this reaction and all three complexes are found to produce good yield of 68-70% but ee 0, 28, 26% respectively (Table 1, entry 14-16). As catalyst **4** is racemic produced no ee, but **4'** gives 28 % ee while the **4"** is 26 % only difference in configuration of the product. Summary of the table 1 is the catalyst **3"** gives better results compared to the other catalyst used in absence of oxygen source. Hence further optimisation of the reaction condition was done by using the catalyst **3"**.

Table 3: Screening of catalyst amount and temperature[a]

[a] All reactions were carried out using 0.5mmol substrate, 3mL of solvents for 72 h. [b] Isolated yield, [c] er and ee were calculated by HPLC profile using Lux cellulose-1 column. [d] NR = No reaction.

In the process of identifying an appropriate solvent, different solvents were tested. Upon varying solvents, the halogenated solvents are found good in producing (Table 2, entry 1-3) maximum yield (≈60-70%), but with poor ee (6-12%) in the case of $CHCl_3$ (Table 2, entry 1), CCl_4 (Table 2, entry 2) and dichloroethane (Table 2, entry 3). All other solvents are found to give poor yield (ranging ≈30 - 45 %) and ee (ranging ≈2-18% in solvents like THF (Table 2, entry 4), methanol (Table 2, entry 5), ethanol (Table 2, entry 6), ethylacetate (Table 2, entry 7), 2-propanol (Table 2, entry 8) and toluene (Table 2, entry 9). However in the case of acetonitrile (Table 2, entry 10), the maximum enantioselectivity upto 40% was observed, although the yield (30%) was not encouraging compared to halogenated solvents. Thus, acetonitrile produce comparatively high ee 40%, but poor yield 30% (Table 2, entry 10). It is noteworthy to mention here that among the halogenated solvents, DCM gives higher yield 75% but poor ee 32% (Table 1; entry 13). Hence assuming the combination of both acetonitrile and DCM to act better solvent, the 1:1 (Table 2, entry 11) and 1:2 binary mixture (Table 2, entry 12) of these solvent mixture were tested. Out of these two, 1:1 ratio gave better yield 60% and the ee was dropped to 24%. Then we used HFIP as solvent, which gave amazing yield of 96% and better ee of 66% (Table 2, entry 13). The results obtained on using HFIP as a solvent although the yield was best, the ee was not appreciable. As acetonitrile producing better enantioselectivity, we used the combination of HFIP and acetonitrile in 1:1 ratio (Table 1, entry 14) which gave significantly good yield (92%) and ee (70%).

Identifying the appropriate solvent, we next examined the amount of catalyst (Table 3, entry 1-9) varying from 0.25 mol% to 10 mol% as shown in table 3. When the amount of catalyst used as 0.25 mol% (Table

3; entry 1), the yield was 70%, but the ee dropped to 56%. Upon increasing the amount of catalyst from 0.5 mol% to 10 mol% (Table 3, entry 2-9), the 2 mol% (Table 3, entry 4) of catalyst gave better yield 96% and the ee raised to 74%. Thus the 2 mol% was fixed as an optimized amount of catalyst.

Then optimize the reaction temperature, we performed the reaction in different temperatures from 0 to 40ºC (Table 3; entry 10-12), and better enantioselectivity was observed at RT (Table 3, entry 4). The reaction at 0ºC gives no conversion of 2-naphthol to BINOL, suggests that the catalyst is not effective at 0ºC (Table 3, entry 12). Hence we moved to high temperature like 35ºC (Table 3; entry 11) which gave conversion of 80% yield and 62% ee. A further increament in tempearture from 35 to 40ºC (Table 3, entry 10) show futher decrease in the yield 75% and ee 40%. Hence we fixed the RT (25±2ºC) as optimised temperature for this reaction.

Chart 1. Oxidative coupling of 2-naphthol substrates[a]

[a] All reactions were carried out using 0.5mmol substrate, 3mL of solvents for 72 h. [b] Isolated yield, [c]ee calculated by UFLC profile using lux cellulose-1 column and amylose-2 column.

Adapting the above optimised conditions, we next screened various substrates with different electron donating and withdrawing groups mainly at 3, 6 and 7th positions of 2-naphthol. From the substrate variation the 2-naphthol (**5a**) produced *R*-BINOL (**6a**) with very good yield of 96 % and excellent ee of 74% ee (Chart 1, **6a**). The 6-bomo-2-naphthol (**5b**) produced (**6b**) with 95% yield and 72% ee (Chart 1, **6b**). The 7-methoxy-2-naphthol (**5c**) produced 7-methoxy BINOL with 92% yield and 70% ee (Chart 1, (**6C**)), likewise 3-bromobinol (Chart 1, **6d**) with 93% yield and 70% ee, 7-bromobinol (Chart 1, **6e**) with 94% yield and 64% ee. The substrate screening the unsubstituted 2-napthol gave highest yield (96%) and ee (74%) that suggest catalyst is interacting well with the unsubstituted one than the substituted 2-naphthol.

Scheme 4. The probable mechanism for the Cu catalysed oxidative coupling reaction.

Based on the understanding gained from the crystal structure and the catalytic performance of the complex 3" in the oxidative coupling a probable mechanism[27] is proposed in scheme 4. Initially in the step-1, the substrate 2-napthol interacts with the Cu(II) of the complex and replace the oxide anion by deprotonation of hydroxyl group to form Cu-naphthalato complex (TS-1). The single electron transfer (SET) process in step 2, reduce the Cu(II) to Cu(I) as shown in TS-2. In the subsequent step 3, the delocalisation of radical generate a resonance form of naphthyloxyl radical TS-3. Two such C-centred napthyloxyl radicals combine together facilitates the C-C coupling by constructing BINOL as shown in step-4 simultaneously regenerate the catalyst by reductive elimination is obvious to understand.

Conclusions

In conclusion, we have demonstrated the synthesis and mechanism of an important terminally closed [**2+2**] double-stranded binuclear helicate-like macrocycle by adapting simple synthetic one-pot approach. In

addition, the spontaneous formation of the interesting species μ_4-oxo-dimer of the dimer, *i.e.* tetramer, **3** was also established with appropriate alteration in the subcomponent ratio. In other words, a simple Schiff base condensation – an age-old synthetic technique – was strategically demonstrated to achieve [**2+2**] helicate-like macrocycles **1** and **1'** by one pot synthesis and a higher order complex **3** had been established. This detailed work confirm that the subcomponent ratio **2:2:2** leads to the synthesis of complex **1**. The change in the subcomponent ratio to **2:4:4**, leads to highly selective formation of complex **3.** Establishing the structure of the **3**, which possess stereochemically favoured four free amine groups, provides a wide range of possibility for the preparation of higher order macrocyclic complexes with variable voids by appropriate selection of aldehydes. The detailed mechanism for the formation of a dimer to tetramer complexes were disclosed for the first time. The DFT energy optimization carried out for complex **1** and **3** suggests the respective relative free energy as ≈87 kcal mol^{-1}, ≈-9 kcal mol^{-1}. The detailed optimization studies carried out for various intermediate species [**Int-1** (≈-1) kcal mol^{-1}), **Int-2** (≈-4 kcal mol^{-1}), **Int-2** (≈89 kcal mol^{-1}) and **Int-4** (≈8 kcal mol^{-1}) involved in the synthesis thus inspired us to propose a feasible mechanism for this diverse complexation process of [**2+2**] helicate, to **2+4**-open frame without any ambiguity. It shows further that the thermodynamically favoured helicate **1** is obtained by refluxing the reaction mixture, whereas at room temperature the reaction mixture provides the μ_4-oxo tetramer **3**. The chiroptical properties of these complexes were thoroughly investigated using extensive circular dichroic spectroscopy. This enantiomerically pure complexes contains Cu(II) center demonsrates the transfer of chirality from ligand to Cu(II) and generates "$\Delta\Delta\Delta\Delta$ and $\Lambda\Lambda\Lambda\Lambda$" geometrical chirality in their respective tetranuclear complexes through self-assembly process. These enantiopure tetranuclear Cu(II) μ_4-oxo complexes were applied in asymmetric oxidative coupling reaction and demonstrated as enanitoselective catalyst giving 96% yield and 74% *ee* in the case of 2-naphthol. We currently working on oxidative coupling reaction to further increase the enantioselectivity of the product by changing the copper instead of iron in the catalyst.

Experimental Section

Materials and methods

4-methyl-2,6-diformylphenol, 4-*tert*-Butyl-2,6-diformylphenol, 1,1'-Binaphyl-2,2'-diamine, (*R*)-(+)-1,1'-Binaphyl-2,2'-diamine, (*S*)-(-)-1,1'-Binaphyl-2,2'-diamine copper acetate monohydrate, Copper(II) chloride dihydrate were purchased from Aldrich & Co. All these chemicals were used as received without any further purification. Microanalyses were done by using a Perkin-Elmer PE 2400 series II CHNS/O elemental analyser. IR spectra were recorded using KBr pellets (1% w/w) on a Perkin-Elmer Spectrum GX FT-IR spectrophotometer. Electronic spectra were recorded on a Shimadzu UV 3101 PC spectrophotometer. Mass analyses were performed using the positive electron spray ionization (ESI^+) technique on a Waters Micromass Q-TOF mass spectrometer. The X-band EPR spectra were recorded using MiniScope MS 5000 - Magnettech - ESR spectrometer. ^1H, ^{13}C NMR, spectra were recorded on a JEOL Delta 600 MHz FT-NMR spectrometer. Chemical shifts for proton resonances are reported in ppm (δ) relative to tetramethylsilane (TMS) and the ^{13}C is related to solvents. The CD spectra were recorded on a JASCO 815 Spectrometer. The enantioselectivity of the monobenzoylated product was determined by UFLC (Shimadzu SCL-10AVP) using chiral columns (Phenomenox Lux cellulose-1 and Amylose-2 column).

Computational section

Optimization and frequency calculations of all the molecules are done at the B3LYP/BS1 level[28] of density functional theory (DFT) using Gaussian 16 program.[29] In BS1, copper center is defined with LANL2DZ basis set and pseudopotentials for core electrons while 6–31G(d) basis set is used to define all other atoms. All the intermediates are characterized by a single imaginary frequency, whereas all the intermediates are confirmed to be a minimum by locating zero imaginary frequency in the vibrational analysis. The Gibbs free energy of every system is estimated by adding the thermal correction to Gibbs free energy calculated at B3LYP/BS1 level. The Gibbs free energies are calculated at the standard reaction conditions, viz. temperature 298.15 K and pressure 1 atm.

General procedure for oxidative coupling reaction of 2-naphthol.

A dry 5 mL flask, equipped with a magnetic stirring bar, was charged with Catalyst **3"** (2 mol %) in HFIP:ACN (1:1 ratio) solvent mixture. Corresponding 2-naphthol (0.5 mmol) were then added successively and the resulting mixture was stirred at RT. The mixture was stirred at the same temperature till the consumption of the substrate. The reaction was monitored by the TLC. After completion of the reaction, the solvent was evaporated by rotavapour. Finally, the crude product was purified by column chromatography (silica gel: 100-200 mesh using ethyl acetate and hexanes) to give the corresponding BINOL(S6). Enantiomeric excess was determined by HPLC using Phenomenox Lux cellulose-1 column and Amylose-2 column using isopropanol and hexanes (10% and 90%) as an eluting agent. The absolute configuration of the BINOL were assigned by comparison HPLC profile with reported literature.[25]

Acknowledgements

CSMCRI communication number CSIR-CSMCRI - 150/2018. Author EC and RA acknowledges the CSIR for SRF grants. The authors gratefully acknowledge DST-SERB New Delhi (Project No. SR/S1/IC-23/2011) for funding. AP kindly acknowledges the Academy of Finland funding (nos. 315911 and 277250). We gratefully acknowledge Prof Markus Albrecht for his valuable suggestions and positive criticism. Members of ADCIF of CSMCRI are acknowledged for their instrumentation support. RSP gratefully acknowledges the DST-SERB Govt. of India, for the financial support by the award of Start-up Research Grant (SERB-SRG) with reference SRG/2019/000912, SRM IST for providing the computational facility.

References

[1] a) V.E. Campbell, X. de Hatten, N. Delsuc, B. Kauffmann, I. Huc, J. R. Nitschke, *Nat. Chem.* **2010**, *2*, 684-687; b) R. A. Bilbeisi, J. K. Clegg, N. Elgrishi, X. de Hatten, M. Devillard, B. Breiner, P. Mal, J. R. Nitschke, *J. Am. Chem. Soc.* **2012**, *134*, 5110-5119; c) A. M. Castilla, W. J. Ramsay and J. R. Nitschke, *Acc. Chem. Res.* **2014**, *47*, 2063-2073.

[2] a) T. Nakamura, H. Kimura, T. Okuhara, M. Yamamura, T. Nabeshima, *J. Am. Chem. Soc.* **2016**, *138*, 794-797; b) S. G. Telfer, T. Sato, R. Kuroda, *Angew. Chem. Int. Ed.* **2004**, *43*, 581-584; c) J. A. Thomas, *Chem. Soc. Rev*. **2007**, *36*, 856-868; d) R. Chakrabarty, P. S. Mukherjee, P. J. Stang, *Chem. Rev*. **2011**, *111*, 6810-6918.

[3] a) C. R. K. Glasson, G. V. Meehan, M. Davies, C. A. Motti, J. K. Clegg, L. F. Lindoy, *Inorg. Chem.* **2015**, *54*, 6986-6992; b) D. F. Perkins, L. F. Lindoy, G. V. Meehan, P. Turner, *Chem. Commun.* **2004**, 152-153; c) D. Black, A. J. Blake, R. L. Finn, L. F. Lindoy, A. Nezhadali, G. Rougnaghi, P. A. Tasker,

M. Schröder, *Chem. Commun*. **2002**, 340-341; d) L. F. Lindoy, K. -M. Park, S. S. Lee, *Chem. Soc. Rev*. **2013**, *42*, 1713-1727.

[4] a) M. Albrecht, *Chem. Rev.* **2001**, *101*, 3457-3498; b) Y. -B. Shu, X. -L. Tang, W. –S. Liu, *Inorg. Chem. Front*. **2014**, *1*, 226-230; c) Y. Suffren, B. Golesorkhi, D. Zare, L. Guénée, H. Nozary, S. V. Eliseeva, S. Petoud, A. Hauser, C. Piguet, *Inorg. Chem.* **2016**, *55*, 9964-9972; d) F. Zhang, A. Fluck, S. A. Baudron, M. W. Hosseini, *Dalton Trans.* **2019**, *48*, 4105-4108; e) H. Houjou, A. Iwasaki, T. Ogihara, M. Kanesato, S. Akaborib, K. Hiratani, *New J. Chem*. **2003**, *27*, 886-889; f) A. Jarzebski, C. Tenten, C. Bannwarth, G. Schnakenburg, S. Grimme, A. Lützen, *Chem. Eur. J.* **2017***, 23*, 12380-12386; g) S. Singh, R. W. Hogue, H. L. C. Feltham, S. Brooker, *Dalton Trans.* **2019**, *48*, 15435-15444; h) F. Artizzu, F. Quochi, A. Serpe, E. Sessinia, P. Deplanoa, *Inorg. Chem. Front*. **2015**, *2*, 213-222.

[5] a) G. Gil-Ramírez, S. Hoekman, M. O. Kitching, D. A. Leigh, I. J. Vitorica-Yrezabal, G. Zhang, *J. Am. Chem. Soc.* **2016**, *138*, 13159-13162; b) J. -F. Ayme, J. E. Beves, D. A. Leigh, R. T. McBurney, K. Rissanen, D. Schultz, *J. Am. Chem. Soc*. **2012**, *134*, 9488-9497; c) J. -F. Ayme, J. E. Beves, C. J. Campbell, D. A. Leigh, *Angew. Chem. Int. Ed.* **2014**, *53*, 7823 -7827; d) A. -F. Ayme, J. E. Beves, C, J. Campbella, D. A. Leigh, *Chem. Soc. Rev.* **2013**, *42*, 1700-1712.

[6] J. Gao, J. H. Reibenspies, R. A. Zingaro, F. R. Wooley, A. E. Martell, A. Clearfield, *Inorg. chem*. **2005**, *44*, 232-241.

[7] a) M. Albrecht, I. Janser, S. Burk, P. Weis, *Dalton trans.* **2006**, *0*, 2875-2880; b) M. A. Pitt, D, W. Johnson, *Chem. Soc. Rev.* **2007**, *36*, 1441-1453; c) M. D. Ward, P. R. Raithby, *Chem. Soc. Rev.* **2013**, *42*, 1619-1636; d) T. Ema, D. Tanida, T. Sakai, *Org. Lett.* **2006**, *8* (17), 3773-3775; e) T. Ema, D. Tanida, K. Hamada, T. Sakai, *J. Org. Chem.* **2008**, *73* (22), 9129-9132.

[8] a) J. -Z. Zhao, T. M. Fyles, T. D. James, *Angew. Chem*. **2004**, *116*, 3543-3546; *Angew. Chem. Int. Ed*. **2004**, *43*, 3461-3464; b) J. Lin, Q. –S. Hu, M. –H. Xu, L. Pu, *J. Am. Chem. Soc*. **2002**, *124*, 2088-2089; c) J. Lin, H. -C. Zhang, L. Pu, *Org. Lett.* **2002**, *4*, 3297-3300; d) Z. –B. Li, J. Lin, H. -C, Zhang, M. Sabat, M. Hyacinth, L. Pu, *J. Org. Chem*. **2004**, *69*, 6284-6293; e) V. Pugh, Q. S. Hu, L. Pu, *Angew. Chem. Int. Ed*. **2000**, *39*, 3638-3641; e) J. Lin, Z. -B, Li, H. -C. Zhang, L. Pu, *Tetrahedron Lett*. **2004**, *45*, 103-106; f) Z. -B. Li, J. Lin, L. Pu, *Angew. Chem. Int. Ed*. **2005**, *44*, 1690-1693.

[9] a) H. Mihara, Y. Xu, N. E. Shepherd, S. Matsunaga, M. Shibasaki, *J. Am. Chem. Soc.* **2009**, *131*, 8384-8385; b) B. Wu, J. C. Gallucci, J. R. Parquette, T. V. RajanBabu, *Angew. Chem., Int. Ed*. **2009**, *48*, 1126-1129; c) T. Yoshino, H. Morimoto, G. Lu, S. Matsunaga, M. Shibasaki, *J. Am. Chem. Soc*. **2009**, *131*, 17068-17069; d) G. Lu, T. Yoshino, H. Morimoto, S. Matsunaga, M. Shibasaki, *Angew. Chem., Int. Ed.* **2011**, *50*, 4382-4385; e) S. Matsunaga, M. Shibasaki, *Chem. Commun.* ***2014***, *50*, 1044-1057.

[10] E. C. Constable, G. Zhang, C. E. Housecroft, M. Neuburger, J. A. Zampese, *Inorg. Chim. Acta.* **2010**, *363(15)*, 4207-4213.

[11] E. Chinnaraja, R. Arunachalam, E. Suresh, S. K. Sen, R. Natarajan, P. S. Subramanian, *Inorg. Chem*. **2019**, *58(7)*, 4465-4479.

[12] a) M. Bera, W. T. Wong, G. Aromi, J. Ribas, D. Ray, *Inorg. Chem.* **2004**, *43*, 4787-4789; b) S. Mukherjee, T. Weyhermuller, E. Bothe, K. Wieghardt, P. Chaudhuri, *Eur. J. Inorg. Chem.* **2003**, 863-875.

[13] E. Chinnaraja, R. Arunachalam, M. K. Choudhary, R. I. Kureshy, P. S. Subramanian, *Appl. Organometal. Chem*. **2016**, *30*, 95-101.

[14] Complex **1'**: CCDC 1850751. Crystal Data for $C_{64}H_{47}Cl_2Cu_2N_7O_2$ (M =1144.06 g/mol): orthorhombic, space group $C222_1$ (no. 20), a = 21.8906(4) Å, b = 27.6915(4) Å, c = 10.79947(17) Å, V = 6546.47(19) Å^3, Z = 4, T = 200.0(1) K, μ(CuKα) = 1.896 mm^{-1}, *Dcalc* = 1.161 g/cm^3, 24816

reflections measured (8.078° ≤ 2Θ ≤ 139.892°), 6204 unique (R_{int} = 0.0475, R_{sigma} = 0.0343) which were used in all calculations. The final R_1 was 0.0478 (I > 2σ(I)) and wR_2 was 0.1227 (all data).

[15] Complex **3**: CCDC 1850752. Crystal Data for $C_{110}H_{88}Cu_4N_{10}O_{11}$ (M =1980.06 g/mol): monoclinic, space group $C2/c$ (no. 15), a = 17.3472(3) Å, b = 29.1579(5) Å, c = 21.7083(4) Å, β = 97.774(2)°, V = 10879.3(3) Å^3, Z = 4, T = 120.0(1) K, μ(CuKα) = 1.357 mm^{-1}, $Dcalc$ = 1.209 g/cm^3, 18406 reflections measured (7.326° ≤ 2Θ ≤ 139.988°), 10244 unique (R_{int} = 0.0255, R_{sigma} = 0.0368) which were used in all calculations. The final R_1 was 0.0446 (I > 2σ(I)) and wR_2 was 0.1249 (all data).

[16] Complex **4**: CCDC 1936526 for $C_{120}H_{106}Cu_4N_{12}O_{11}$ (M =2146.32 g/mol): monoclinic, space group C2/c (no. 15), a = 31.6514(7) Å, b = 12.6358(3) Å, c = 26.3332(7) Å, β = 90.092(2)°, V = 10531.7(5) Å^3, Z = 4, T = 120.00(10) K, μ(CuKα) = 1.449 mm^{-1}, $Dcalc$ = 1.354 g/cm^3, 20902 reflections measured (7.534° ≤ 2Θ ≤ 139.99°), 9935 unique (R_{int} = 0.0275, R_{sigma} = 0.0368) which were used in all calculations. The final R_1 was 0.0418 (I > 2σ(I)) and wR_2 was 0.1175 (all data).

[17] a) E. Chinnaraja, R. Arunachalam, J. Samanta, R. Natarajan, P. S. Subramanian, *Appl. Organometal. Chem.* **2019**, *33,* e4827; b) E. Chinnaraja, R. Arunachalam, K. Samanta, R. Natarajan, P. S. Subramanian, *Adv. Synth. Catal*. 10.1002/adsc.201901350; c) M. Seitz, S. Stempfhuber, M. Zabel, M. Schütz, O. Reiser, *Angew Chem., Int Ed*. **2005**, *44*, 242-245; d) H. Miyasaka, S. Okamura, T. Nakashima, N. Matsumoto, *Inorg. Chem.* **1997**, *36,* 4329-4335; 4) P. M. Selvakumar, E. Suresh, P.S. Subramanian, *Polyhedron*. **2009**, *28*, 245–252.

[18] a) M. Hutin, C. J. Cramer, L. Gagliardi, A. R. M. Shahi, G. Bernardinelli, R. Cerny, J. R. Nitschke, *J. Am. Chem. Soc*. **2007**, *129*, 8774-8780; b) O. Gidron, M. Jirásek, N. Trapp, M. -O. Ebert, X. Zhang, F. Diederich, *J. Am. Chem. Soc*. **2015**, *137*, 12502-12505; c) H. Jędrzejewska, A. Szumna, *Chem. Rev.* **2017**, *117*, 4863-4899; d) M. L. Saha, M. Schmittel, *Org. Biomol. Chem.* **2012**, *10*, 4651-4684; e) C. Dressel, T. Reppe, M. Prehm, M. Brautzsch, C. Tschierske, *Nat. Chem*. **2014**, *6*, 971-977; f) L. R. Holloway, P. M. Bogie, R. J. Hooley, *Dalton Trans.* **2017**, *46*, 14719-14723.

[19] a) P. S. Subramanian, E. Suresh, D. Srinivas, *Inorg. Chem.* **2000**, *39,* 2053; b) A. Ozarowski, I. B. Szymańska, T. Muzioł, J. Jezierska, *J. Am. Chem. Soc.* **2009**, *131*, 10279-10292; c) D. Das, Y. -M, Lee, K. Ohkubo, W. Nam, K. D. Karlin, S. Fukuzumi, *J. Am. Chem. Soc.* **2013**, *135*, 4018-4026.

[20] G. Alzuet, L. Casella, M. L. Villa, O. Carugo, M. Gullotti, *J. Chem. Soc., Dalton Trans.* **1997**, 4789-4794.

[21] M. Sarkar, R. Clérac, C. Mathoniére, N. G. R. Hearns, V. Bertolasi, D. Ray, *Inorg. Chem*. **2011**, *50*, 3922-3933.

[22] J. Gao, J. H. Reibenspies, A. E. Martell, *Angew. Chem. Int. Ed.* **2003***, 42,* 6008-6012.

[23] U. A. Kshirsagar, C. Regev, R. Parnes, D. Pappo, *Org. Lett.* **2013**, *15*, 3174-3177.

[24] S. Takizawa, T. Katayama, C. Kameyama, K. Onitsuka, T. Suzuki, T. Yanagida, T. Kawai, H. Sasai*, Chem. Commun.* **2008**, 1810-1812.

[25] a) S. Natrute, R. Parenes, F. D. Toste, D. Pappo, *J. Am. Chem*. **2016**, *138*, 16553-16560; b) A. Libman, H. Shalit, Y. Vainer, S. Narute, S. Kozuch, D. Pappo, *J. Am. Chem. Soc.* **2015***, 37*, 11453-1460.

[26] a) B. Feringa, H. Wynberg, *Bioorg. Chem.* **1978***, 7*, 397-408; b) J. Brussee, A. C. A. Jansen, *Tetrahedron Lett.* **1983**, *24*, 3261-3262; c) M. Smrcina, M. Lorenc, V. Hanus, P. Sedmera, P. Kocovsky, *J. Org. Chem.* **1992***, 57,* 1917-1920; d) M. Smrcina, J. Polakova, S. Vyskocil, P. Kocovsky, *J. Org. Chem.* **1993**, *58*, 4534-4538; e) M. Nakajima, I. Miyoshi, K. Kanayama, S. I. J. Hashimoto, *Org. Chem.* **1999**, *64*, 2264-2271; f) M. Noji, M. Nakajima, K. Koga, *Tetrahedron Lett*. **1994**, *35*, 7983-7984; g) S. K. Alamsetti, E. Poongulazhuli, D. Ganaphathy, G. Sekar, *Adv. synth. Catal.* **2013**, *355*, 2803-2808.

[27] P. Adão, S. Barroso, M. F. N. N. Carvalho, C. M. Teixeira, M. L. Kuznetsov, J. C. Pessoa, *Dalton Trans*. **2015**, *44*, 1612-1626.

[28] a) A. D. Becke, *J. Chem. Phys.* **1993**, *98,* 5648-5652; b) C. T. Lee, W. T. Yang, R. G. Parr, *Phys. Rev. B.* **1988**, *37*, 785-789.

[29] Gaussian 16, Revision B.01, M. J. Frisch, G. W. Trucks,H. B. Schlegel, G. E. Scuseria, M. A. Robb, J. R. Cheeseman, G. Scalmani, V. Barone, G. A. Petersson, H. Nakatsuji, X. Li, M. Caricato, A. V. Marenich, J. Bloino, B. G. Janesko, R. Gomperts, B. Mennucci, H. P. Hratchian, J. V. Ortiz, A. F. Izmaylov, J. L. Sonnenberg, D. Williams-Young, F. Ding, F. Lipparini,F. Egidi, J. Goings, B. Peng, A. Petrone, T. Henderson, D. Ranasinghe, V. G. Zakrzewski, J. Gao, N. Rega, G. Zheng, W. Liang, M. Hada, M. Ehara, K. Toyota, R. Fukuda, J. Hasegawa, M. Ishida, T. Nakajima, Y. Honda, O. Kitao, H. Nakai, T. Vreven, K. Throssell, J. A. Jr. Montgomery, J. E. Peralta, F. Ogliaro, M. J. Bearpark, J. J. Heyd, E. N. Brothers, K. N. Kudin, V. N. Staroverov, T. A. Keith, R. Kobayashi, J. Normand, K. Raghavachari,A. P. Rendell, J. C. Burant, S. S. Iyengar, J. Tomasi, M. Cossi, J. M. Millam, M. Klene, C. Adamo, R. Cammi, J. W. Ochterski,R. L. Martin, K. Morokuma, O. Farkas, J. B. Foresman, D. J. Fox, *Gaussian, Inc., Wallingford CT*, **2016**.

Table 1: Screening of catalyst and oxidising agent[a]

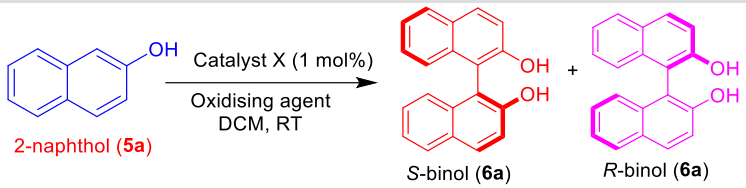

Entry	Catalyst	Oxidising agent	Yield[b] %	er[c]% (S:R)	ee[c] %
1	**1**	Air	20	50:50	--
2	**1'**	Air	25	56:44	12(*S*)
3	**2**	Air	23	50:50	--
4	**2'**	Air	26	55:45	10(*S*)
5	**3**	Air	50	50:50	--
6	**3'**	Air	52	60:40	20(*S*)
7	**3'**	t-BuOOt-Bu	60	53:47	6(*S*)
8	**3'**	t-BuOOH[d]	54	55:45	10(*S*)
9	**3'**	t-BuOOH [e]	58	51:49	2(*S*)
10	**3'**	H_2O_2	55	53:47	6(*S*)
11	**3'**	O_2	56	55:45	10(*S*)
12	**3'**	--	74	65:35	30(*S*)
13	**3"**	--	75	34:66	32(*R*)
14	**4**	--	70	50:50	--
15	**4'**	--	68	64:36	28(*S*)
16	**4"**	--	69	37:63	26(*R*)

[a] All reactions were carried out using 0.5mmol substrate, 3mL of solvents for 72 h. [b] Isolated yield, [c] er and ee were calculated by HPLC profile using Lux cellulose-1 column. Configuration of the product was assigned by comparing with HPLC profile of reported. [d]t-BuOOH in H_2O. [e]t-BuOOH in decane.

Table 2: Solvent variation[a]

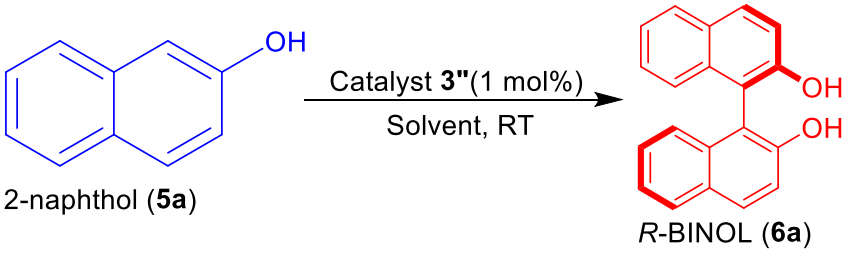

Entry	Solvent	Yield[b] %	er[c]% (S:R)	ee[c] % (*R*)
1	$CHCl_3$	70	44:56	12
2	CCl_4	60	47:53	6
3	$ClCH_2CH_2Cl$	65	44:56	12
4	THF	45	47:53	6
5	CH_3OH	40	49:51	2
6	EtOH	38	47:53	6
7	EtOAc	30	48:52	4
8	$CH_3CH(OH)CH_3$	38	49:51	2
9	$C_6H_5CH_3$	37	41:59	18
10	CH_3CN	30	30:70	40
11	CH_2Cl_2: CH_3CN (1:1)	60	38:62	24
12	CH_2Cl_2: CH_3CN (1:2)	40	41:59	18
13	HFIP	96	17:83	66
14	HFIP:CH_3CN (1:1)	92	15:85	70

[a] All reactions were carried out using 0.5mmol substrate, 3mL of solvents for 72 h. [b] Isolated yield, [c] er and ee were calculated by HPLC profile using Lux cellulose-1 column.

Table 3: Screening of catalyst amount and temperature[a]

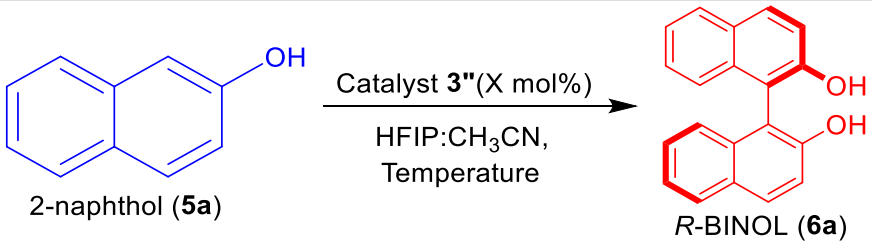

2-naphthol (**5a**) *R*-BINOL (**6a**)

Entry	Amount of catalyst (mol%)	Temp °C	Yield[b] %	er[c]% (*S:R*)	ee[c] % (*R*)
1	0.25	RT	70	22:78	56
2	0.5	RT	85	20:80	60
3	1.5	RT	94	18:82	64
4	2	RT	96	13:87	74
5	2.5	RT	94	15:85	70

6	3	RT	94	19:81	62
7	5	RT	90	19:81	62
8	7	RT	88	22:78	56
9	10	RT	87	25:75	50
10	2	40	75	30:70	40
11	2	35	80	19:81	62
12	2	0	NR[d]	NR	NR

[a] All reactions were carried out using 0.5mmol substrate, 3mL of solvents for 72 h. [b] Isolated yield, [c] er and ee were calculated by HPLC profile using Lux cellulose-1 column. [d] NR = No reaction.

Received: ((will be filled in by the editorial staff))
Published online:((will be filled in by the editorial staff))